C_{60} Dimers: A Route to Endohedral Fullerene Compounds?

Serguei Patchkovskii and Walter Thiel*

Contribution from the Organisch-chemisches Institut, Universität Zürich, Winterthurerstrasse 190, CH-8057 Zürich, Switzerland

Received July 21, 1997. Revised Manuscript Received November 13, 1997

Abstract: An autocatalytic mechanism for helium incorporation into buckminsterfullerene has been examined by MNDO, density functional theory (DFT), and ab initio calculations. The mechanism involves dimerization of two molecules by [2+2] cycloaddition between double bonds at hexagon junctions, formation of a stable closed-shell window, and helium insertion through this window. According to MNDO, the activation barriers do not exceed 100 kcal/mol for any of these steps. At the DFT level, the window isomer is kinetically less stable and may therefore be mechanistically less relevant. Even in this case, the effective DFT activation barrier for helium incorporation into the [2+2] dimer is around 130 kcal/mol, much lower than for buckminsterfullerene itself. Vibrational and NMR spectra are predicted for the proposed window dimer to facilitate its experimental detection. The applicability of the dimer mechanism to other noble gases and to higher fullerenes is also discussed, as well as possible variants involving helium incorporation by C_{60} polymers and by tethered C_{60} dimers.

Introduction

He@C_{60} has been produced by high-energy collisions in a mass spectrometer[1−5] and by heating buckminsterfullerene in a helium atmosphere.[6] Macroscopic amounts of this and other endohedral fullerenes with a noble gas atom inside can be produced using high pressure[7−9] or beam implantation.[10] Endohedral labeling with the NMR-active ^{3}He isotope provides an important tool in studies of fullerene structure[8,9,11,12] and reactivity.[13−16] Practical applications of these endohedral fullerenes are hampered by the very low yields obtainable in the high-pressure synthesis, which usually do not exceed a few tenths of a percent.[7−10] Equilibrium yields higher by 1−2 orders of magnitude are predicted from estimates of the available volume,[6] model potential studies,[17] and accurate ab initio computations[18] (at the typical reaction conditions, 600 °C and 3000 atm). Since incorporation of noble gases appears to be kinetically limited, knowledge of the reaction mechanism is necessary to improve the yields.

A window mechanism, where a bond in C_{60} is broken reversibly to allow an easy passage of a guest, has been proposed[6,19] in order to explain the experimental results. However, an exhaustive study of all mechanistically relevant one- and two-bond windows in buckminsterfullerene[20] has found barriers for helium insertion in excess of 200 kcal/mol for each of the 21 possible pathways. Activation barriers of this magnitude can be overcome in mass-spectroscopic[1−5] and beam[10] experiments, but not under the high-pressure conditions.[7−9]

Impurities have been suggested to play an important role in noble gas incorporation,[20,21] and a study of neon release from Ne@C_{60} has found a strong dependence of the noble gas release rate on the sample purity.[21] A recent theoretical study[22] has examined how the addition of either one or two radicals X (modeled by H and CH_3) affects the activation barriers for helium incorporation. These barriers are decreased significantly when X is added to one, or both, of the atoms from the bond that is broken to form the window. However, even the lowest barriers obtained (ca. 160 kcal/mol for $C_{60}CH_3$, 130−140 kcal/mol for $C_{60}(CH_3)_2$ isomers) are still too high to account for noble gas inclusion. It remains unclear whether these barriers might be even lower for other radicals X, and also which impurities are actually involved (not yet identified experimentally).

(1) Weiske, T.; Böhme, D. K.; Hrušák, J.; Krätschmer, W.; Schwarz, H. *Angew. Chem., Int. Ed. Engl.* **1991**, *30*, 884−886.
(2) Ross, M. M.; Callahan, J. H. *J. Phys. Chem.* **1991**, *95*, 5720−5723.
(3) Caldwell, K. A.; Giblin, D. E.; Hsu, C. S.; Cox, D.; Gross, M. L. *J. Am. Chem. Soc.* **1991**, *113*, 8519−8521.
(4) Weiske, T.; Wong, T.; Krätschmer, W.; Terlouw, J. K.; Schwarz, H. *Angew. Chem., Int. Ed. Engl.* **1992**, *31*, 183−185.
(5) Schwarz, H.; Weiske, T.; Böhme, D. K.; Hrušák, J. In *Buckminsterfullerenes*; Billups, W. E., Cuifolini, M. A., Eds.; VCH: New York, 1993; pp 257−283.
(6) Saunders, M.; Jiménez-Vázquez, H. A.; Cross, R. J.; Poreda, R. J. *Science* **1993**, *259*, 1428−1430.
(7) Saunders, M.; Jiménez-Vázquez, H. A.; Cross, R. J.; Mroczkowski, S.; Gross, M. L.; Giblin, D. E.; Poreda, R. J. *J. Am. Chem. Soc.* **1994**, *116*, 2193-2194.
(8) Saunders, M.; Jiménez-Vázquez, H. A.; Cross, R. J.; Mroczkowski, S.; Freedberg, D. I.; Anet, F. A. L. *Nature* **1994**, *367*, 256−258.
(9) Saunders, M.; Cross, R. J.; Jiménez-Vázquez, H. A.; Shimshi, R.; Khong, A. *Science* **1996**, *271*, 1693−1697.
(10) Shimshi, R.; Cross, R. J.; Saunders, M. *J. Am. Chem. Soc.* **1997**, *119*, 1163−1164.
(11) Saunders, M.; Jiménez-Vázquez, H. A.; Cross, R. J.; Billups, W. E.; Gesenberg, C.; Gonzalez, A.; Luo, W.; Haddon, R. C.; Diederich, F.; Herrmann, A. *J. Am. Chem. Soc.* **1995**, *117*, 9305−9308.
(12) Bühl, M.; van Wüllen, C. *Chem. Phys. Lett.* **1995**, *247*, 63−68.
(13) Smith, A. B.; Strongin, R. M.; Brard, L.; Furst, G. T.; Atkins, J. H.; Romanow, W. J.; Saunders, M.; Jiménez-Vázquez, H. A.; Owens, K. G.; Goldschmidt, R. J. *J. Org. Chem.* **1996**, *61*, 1904−1905.
(14) Schuster, D. I.; Cao, J.; Kaprinidis, N.; Wu, Y.; Jensen, A. W.; Lu, Q.; Wang, H.; Wilson, S. R. *J. Am. Chem. Soc.* **1996**, *118*, 5639−5647.
(15) Cross, R. J.; Jiménez-Vázquez, H. A.; Lu, Q.; Saunders, M.; Schuster, D. I.; Wilson, S. R.; Zhao, H. *J. Am. Chem. Soc.* **1996**, *118*, 11454−11459.
(16) Billups, W. E.; Gonzalez, A.; Gesenberg, C.; Luo, W.; Marriott, T.; Alemany, L. B.; Saunders, M.; Jiménez-Vázquez, H. A.; Khong, A. *Tetrahedron Lett.* **1997**, *38*, 175−178.
(17) Jiménez-Vázquez, H. A.; Cross, R. J. *J. Chem. Phys.* **1996**, *104*, 5589−5593.
(18) Patchkovskii, S.; Thiel, W. *J. Chem. Phys.* **1997**, *106*, 1796−1799.
(19) Murry, R. L.; Scuseria, G. E. *Science* **1994**, *263*, 791−793.
(20) Patchkovskii, S.; Thiel, W. *J. Am. Chem. Soc.* **1996**, *118*, 7164−7172.
(21) Shimshi, R.; Khong, A.; Jiménez-Vázquez, H. A.; Cross, R. J.; Saunders, M. *Tetrahedron* **1996**, *52*, 5143−5148.
(22) Patchkovskii, S.; Thiel, W. *Helv. Chim. Acta* **1997**, *80*, 495−509.

S0002-7863(97)02456-6 CCC: $15.00
Published on Web 01/07/1998

The lack of a convincing mechanistic interpretation for the high-pressure experiments[7−9] leads us to consider a process for noble gas incorporation involving catalysis by the most abundant species in C_{60} samples: buckminsterfullerene itself. The propensity of buckminsterfullerene to undergo a reversible polymerization upon irradiation with UV or visible light,[23,24] as well as during a high-pressure−high-temperature treatment,[25] is well-known. Several distinct polymerized C_{60} phases have been prepared, including predominantly dimers,[26] branched oligomers,[24,26] small 3D clusters,[27] linear polymers,[28−30] and several two-dimensional polymers.[29] Slow pressure-induced polymerization has been observed under conditions similar to those employed in the high-pressure synthesis of endohedral fullerenes (e.g., 200 °C, 8000 atm[28]). In most polymerized phases the local binding is consistent with a [2+2] cycloaddition between double bonds at hexagon junctions in C_{60},[26−36] irrespective of the exact synthesis conditions. The polymers revert to the pristine buckminsterfullerene upon heating above 270 °C[25,26] at normal pressure. The depolymerization process is either thermoneutral or slightly endothermic,[25,28] depending on the sample preparation. Recently, a solid-state synthesis of the pure C_{60} dimer has been reported in the literature.[37]

Dimers, oligomers, and polymers of buckminsterfullerene **1** have also enjoyed considerable theoretical attention.[38−47] Although little agreement exists on the absolute heat of C_{60} dimerization, the D_{2h} isomer **2** (see Figure 1), the product of the [2+2] cycloaddition between two double bonds at hexagon junctions, is predicted to have the lowest energy compared to other [2+2] adducts,[38,39,41,42] [4+4] adducts,[41] and single-bonded isomers.[43,44] The dimer **2** contains elongated intra-fullerene "hinge" bonds in the connecting cyclobutane ring, which are expected to dissociate easily to form the window isomer **3**[41,45] (see Figure 1). This isomer has been proposed as a likely intermediate in coalescence to "buckypeanuts" and higher fullerenes.[41,47] The striking similarity between **3** and the window structures examined previously as possible conduits for helium insertion[19,20,22] suggests the following autocatalytic mechanism for noble gas incorporation (see Figure 1 for the structures of **2**−**5**):

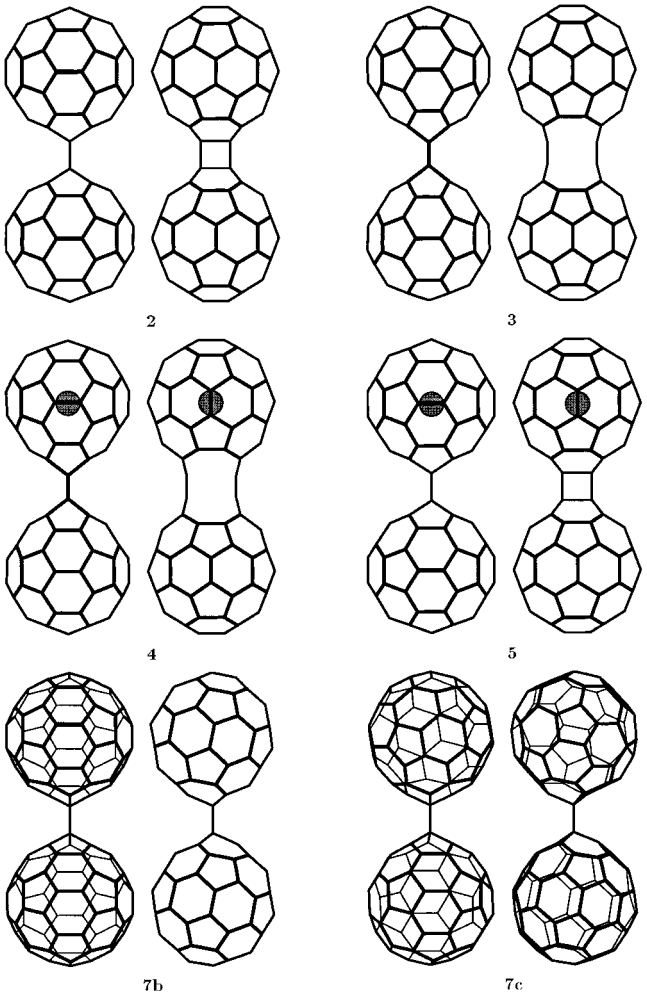

Figure 1. Optimized MNDO geometries for the stable intermediates in the helium incorporation process. For each structure, left and front views are given.

$$2C_{60}\,(\mathbf{1}) \longrightarrow C_{60}{=}C_{60}\,(\mathbf{2}) \qquad \text{(I)}$$

$$C_{60}{=}C_{60}\,(\mathbf{2}) \longrightarrow C_{60}\overset{\frown}{}C_{60}\,(\mathbf{3}) \qquad \text{(II)}$$

$$C_{60}\overset{\frown}{}C_{60}\,(\mathbf{3}) + He \longrightarrow He@C_{60}\overset{\frown}{}C_{60}\,(\mathbf{4}) \qquad \text{(III)}$$

$$He@C_{60}\overset{\frown}{}C_{60}\,(\mathbf{4}) \longrightarrow He@C_{60}{=}C_{60}\,(\mathbf{5}) \qquad \text{(IV)}$$

$$He@C_{60}{=}C_{60}\,(\mathbf{5}) \longrightarrow He@C_{60}\,(\mathbf{6}) + C_{60}\,(\mathbf{1}) \qquad \text{(V)}$$

The present paper reports a detailed theoretical study of each of the reaction steps I−V. Possible alternatives to the C_{60}

(23) Zhou, P.; Rao, A. M.; Wang, K.-A.; Robertson, J. D.; Eloi, C.; Meier, M. S.; Ren, S. L.; Bi, X.-X.; Eklund, P. C. *Appl. Phys. Lett.* **1992**, *60*, 2871−2873.
(24) Rao, A. M.; Zhou, P.; Wang, K.-A.; Hager, G. T.; Holden, J. M.; Wang, Y.; Lee, W.-T.; Bi, X.-X.; Eklund, P. C.; Cornett, D. S.; Duncan, M. A.; Amster, I. J. *Science* **1993**, *259*, 955−957.
(25) Iwasa, Y.; Arima, T.; Fleming, R. M.; Siegrist, T.; Zhou, O.; Haddon, R. C.; Rothberg, L. J.; Lyons, K. B.; Carter, H. L., Jr.; Hebard, A. F.; Tycko, R.; Dabbagh, G.; Krajewski, J. J.; Thomas, G. A.; Yagi, T. *Science* **1994**, *264*, 1570−1572.
(26) Burger, B.; Winter, J.; Kuzmany, H. *Z. Phys. B* **1996**, *101*, 227−233.
(27) Sun, Y.-P.; Ma, B.; Bunker, C. E.; Liu, B. *J. Am. Chem. Soc.* **1995**, *117*, 12705−12711.
(28) Sundqvist, B.; Andersson, O.; Edlund, U.; Fransson, Å.; Inaba, A.; Jacobsson, P.; Johnels, D.; Launois, P.; Meingast, C.; Moret, R.; Moritz, T.; Persson, P.-A.; Soldatov, A.; Wågberg, T. In *Fullerenes*; Kadish K. M., Ruoff R. S., Eds.; Electrochemical Society: Pennington, 1996; Vol. 3, pp 1014−1028.
(29) Núñez-Regueiro, M.; Marques, L.; Hodeau, J. L.; Béthoux, O.; Perroux, M. *Phys. Rev. Lett.* **1995**, *74*, 278−281.
(30) Agafonov, V.; Davydov, V. A.; Kashevarova, L. S.; Rakhmanina, A. V.; Kahn-Harari, A.; Dubois, P.; Céolin, R.; Szwarc, H. *Chem. Phys. Lett.* **1997**, *267*, 193−198.
(31) Zhou, P.; Dong, Z.-H.; Rao, A. M.; Eklund, P. C. *Chem. Phys. Lett.* **1993**, *211*, 337−340.
(32) Goze, C.; Rachdi, F.; Hajji, L.; Núñez-Regueiro, M.; Marques, L.; Hodeau, J.-L.; Mehring, M. *Phys. Rev. B* **1996**, *54*, R3676−R3678.
(33) Persson, P.-A.; Edlund, U.; Jacobsson, P.; Johnels, D.; Soldatov, A.; Sundqvist, B. *Chem. Phys. Lett.* **1996**, *258*, 540−546.
(34) Wågberg, T.; Persson, P.-A.; Sundqvist, B.; Jacobsson, P. *Appl. Phys. A* **1997**, *64*, 223−226.
(35) Rachdi, F.; Goze, C.; Hajji, L.; Thier, K. F.; Zimmer, G.; Mehring, M.; Núñez-Regueiro, M. *Appl. Phys. A* **1997**, *64*, 295−299.
(36) Rao, A. M.; Eklund, P. C.; Venkateswaran, U. D.; Tucker, J.; Duncan, M. A.; Bendele, G. M.; Stephens, P. W.; Hodeau, J.-L.; Marques, L.; Núñez-Regueiro, M.; Bashkin, I. O.; Ponyatovsky, E. G.; Morovsky, A. P. *Appl. Phys. A* **1997**, *64*, 231−239.
(37) Wang, G.-W.; Komatsu, K.; Murata, Y.; Shiro, M. *Nature* **1997**, *387*, 583−586.
(38) Strout, D. L.; Murry, R. L.; Xu, C.; Eckhoff, W. C.; Odom, G. K.; Scuseria, G. E. *Chem. Phys. Lett.* **1993**, *214*, 576−582.
(39) Adams, G. B.; Page, J. B.; Sankey, O. F.; O'Keeffe, M. *Phys. Rev. B* **1994**, *50*, 17471−17479.
(40) Xu, C. H.; Scuseria, G. E. *Phys. Rev. Lett.* **1995**, *74*, 274−277.
(41) Ōsawa, S.; Ōsawa, E.; Hirose, Y. *Fullerene Sci. Technol.* **1995**, *3*, 565−585.
(42) Porezag, D.; Pederson, M. R.; Frauenheim, Th.; Köhler, Th. *Phys. Rev. B* **1995**, *52*, 14963−14970.
(43) Kürti, J.; Németh, K. *Chem. Phys. Lett.* **1996**, *256*, 119−125.
(44) Scuseria, G. E. *Chem. Phys. Lett.* **1996**, *257*, 583−586.

dimerization (step I) and the relevance of the proposed mechanism for higher fullerenes are also discussed.

Computational Methods

The computational methods employed were the same as in our previous studies:[20,22] MNDO with standard parameters[48,49] and density-functional theory (DFT)[50] using the 3-21G basis set[51] along with the gradient-corrected BLYP[52−54] functional. For the key structures **2** and **3**, AM1[55] and PM3[56] semiempirical, as well as LDA,[52] BP86,[52,53,57] B3LYP,[58] and ab initio Hartree−Fock[51] calculations were carried out to examine the sensitivity of the results to the choice of the computational model. The basis set dependence of the BLYP results was explored using the 6-311G(d) basis set.[59]

At the semiempirical level, the geometries of all structures were fully optimized and characterized as minima, transition structures, or higher-order saddle points by vibrational analysis. Unless noted otherwise, single-point DFT computations were performed at the resulting MNDO geometries. In a few cases, structures were fully optimized at the DFT level, but no characterization of the nature of the stationary points was attempted due to the excessive cost of such computations.

The [2+2] cycloaddition reactions I and V, as well as the window-opening reactions II and IV, involve changes in orbital occupations, so that the corresponding transition structures cannot be described adequately at the single-configuration SCF level. A qualitatively correct description may be provided[60] by the unrestricted Hartree−Fock (UHF)[61] approach, or by configuration interaction (CI), among other possibilities.[51] At the MNDO level, the UHF formulation suffers from spurious spin polarization, and cannot be meaningfully applied to fullerenes.[20] The minimal 3×3 CI involving partially occupied orbitals of the half-electron open-shell singlet reference configuration,[60] on the other hand, produces qualitatively correct results, and was used for the reactions I, II, IV, and V. DFT computations of the transition structures and intermediates in these reactions employed spin-unrestricted singlet wave functions, since they do not suffer from excessive spin contamination.

For **2** and **3**, ^{13}C NMR chemical shifts were computed using the ab initio GIAO−RHF method[62,63] with the 3-21G basis set, and the exploratory GIAO−MNDO parametrization ("method A")[64] with an STO-4G expansion of the three-center terms.[65] This parametrization exhibits an rms deviation of 12.6 ppm from the experimental ^{13}C chemical shifts for 299 common organic molecules (691 individual shift values).[64]

Table 1. Relative Energies and Heats of Formation for the C_{60} Dimer **2** and Its Window Isomer **3**

	ΔE^a (kcal/mol)	$R_a{}^b$ (Å)	$R_b{}^c$ (Å)
Dimer **2**			
exptl[69]	−48.2[d]		
exptl[25,28]	∼0.0[e]		
exptl[34]	≥−21.0[f]		
exptl[72]	≥−29.0[g]		
exptl[37]		1.575[h]	1.581[h]
MNDO[44]	−49.1	1.560	1.616
AM1[41]	−33.1	1.546	1.603
PM3[43]	−37.0	1.549	1.598
RHF/3-21G[44]	−10.4	1.575	1.594
DF-TB[42]	−4.6	1.583	1.590
PW GGA-II/(5s4p)//DF-TB[42]	−7.4		
LDA/3-21G[44]	−30.0	1.575	1.585
BLYP/3-21G	8.2	1.612	1.624
B3LYP/3-21G[44]	5.1	1.594	1.606
RHF/3-21G//MNDO	−10.1		
LDA/3-21G//MNDO	−17.6		
B3LYP/3-21G//MNDO	3.6		
BLYP/3-21G//MNDO	11.6		
BP86/3-21G//MNDO	2.5		
BLYP/6-311G(d)//MNDO	17.3		
Window **3**			
MNDO	−13.4	1.348	2.816
AM1[41]	2.4	1.336	2.648
PM3	10.7	1.336	2.666
BLYP/3-21G	69.9	1.349	2.693
RHF/3-21G//MNDO	71.0		
LDA/3-21G//MNDO	64.7		
B3LYP/3-21G//MNDO	75.1		
BLYP/3-21G//MNDO	75.5		
BP86/3-21G//MNDO	75.6		
BLYP/6-311G(d)//MNDO	66.2		

[a] Energies and heats of formation relative to two noninteracting C_{60} molecules at the same level. Total energies and heats of formation are available as Supporting Information. [b] Length of the connecting pivot bonds of the cyclobutane bridge in **2**, corresponding C═C bond length in **3**. [c] Length of the intra-C_{60} hinge bonds of the cyclobutane bridge in **2**, corresponding CC distance in **3**. [d] Determined from the temperature dependence of the gas-phase equilibrium constant, estimated error of 2.8 kcal/mol. The interpretation as heat of C_{60} dimerization is uncertain due to the lack of pressure-dependent data.[70] [e] Constraint from the heat of depolymerization of high-pressure C_{60} phases. [f] Constraint from the apparent activation energy for depolymerization of C_{60} photopolymers. [g] Constraint from the apparent activation energy for depolymerization of high-pressure C_{60} phases. [h] Determined from X-ray crystallography. Estimated error of 0.007 Å.

All semiempirical computations were performed with the MNDO94 program,[66] modified to include analytical CI gradients[67] and the GIAO evaluation of the NMR shielding tensors.[64,65] All ab initio and DFT computations were performed with the Gaussian94 program.[68]

Results

Table 1 summarizes theoretical and experimental results for the dimer **2** and its window isomer **3** (see also Figure 1). According to all methods employed in the present study, the bonds in the connecting cyclobutane ring of **2** are slightly elongated compared to a typical single bond, with the intra-fullerene ("hinge") bonds somewhat longer than the connecting

(45) Õsawa, S.; Sakai, M.; Õsawa, E. *J. Phys. Chem. A* **1997**, *101*, 1378−1383.
(46) Stafström, S.; Fagerström, J. *Appl. Phys. A* **1997**, *64*, 307−314.
(47) Honda, K.; Õsawa, E.; Slanina, Z.; Matsumoto, T. *Fullerene Sci. Technol.* **1996**, *4*, 819−834.
(48) Dewar, M. J. S.; Thiel, W. *J. Am. Chem. Soc.* **1977**, *99*, 4899−4907, 4907−4917.
(49) Kolb, M.; Thiel, W. *J. Comput. Chem.* **1993**, *14*, 37−44.
(50) Parr, R. G.; Yang, W. *Density-Functional Theory of Atoms and Molecules*; Oxford University Press: Oxford, 1989.
(51) Hehre, W. J.; Radom, L.; Schleyer, P.v.R.; Pople, J. A. *Ab Initio Molecular Orbital Theory*; Wiley: New York, 1986.
(52) Vosko, S. H.; Wilk, L.; Nusair, M. *Can. J. Phys.* **1980**, *58*, 1200−1211.
(53) Becke, A. D. *Phys. Rev. A* **1988**, *38*, 3098−3100.
(54) Lee, C.; Yang, W.; Parr, R. G. *Phys. Rev. B* **1988**, *37*, 785−789.
(55) Dewar, M. J. S.; Zoebisch, E. G.; Healy, E. F.; Stewart, J. J. P. *J. Am. Chem. Soc.* **1985**, *107*, 3902−3909.
(56) Stewart, J. J. P. *J. Comput. Chem.* **1989**, *10*, 209−220, 221−264.
(57) Perdew, J. P. *Phys. Rev. B* **1986**, *33*, 8822−8824; **1986**, *34*, 7406.
(58) Becke, A. D. *J. Chem. Phys.* **1993**, *98*, 5648−5652.
(59) Krishnan, R.; Binkley, J. S.; Seeger, R.; Pople, J. A. *J. Chem. Phys.* **1980**, *72*, 650−654.
(60) Dewar, M. J. S.; Olivella, S.; Stewart, J. J. P. *J. Am. Chem. Soc.* **1986**, *108*, 5771−5779.
(61) Pople, J. A.; Nesbet, R. K. *J. Chem. Phys.* **1954**, *22*, 571−572.
(62) Ditchfield, R. *Mol. Phys.* **1974**, *27*, 789−807.
(63) Wolinski, K.; Hinton, J. F.; Pulay, P. *J. Am. Chem. Soc.* **1990**, *112*, 8251−8260.
(64) Patchkovskii, S. Analytical Computation of First-Order Response Properties in MNDO Methods. Ph.D. Thesis, University of Zürich, 1997.
(65) Patchkovskii, S.; Thiel, W. Manuscript in preparation.
(66) Thiel W. Program MNDO94, version 4.0, 1994.
(67) Patchkovskii, S.; Thiel, W. *Theor. Chem. Acc.* **1997**, *98*, 1−4.
(68) Frisch, M. J.; Trucks, G. W.; Schlegel, H. B.; Gill, P. M. W.; Johnson, B. G.; Robb, M. A.; Cheeseman, J. R.; Keith, T.; Petersson, G. A.; Montgomery, J. A.; Raghavachari, K.; Al-Laham, M. A.; Zakrzewski, V. G.; Ortiz, J. V.; Foresman, J. B.; Peng, C. Y.; Ayala, P. Y.; Chen, W.; Wong, M. W.; Andres, J. L.; Replogle, E. S.; Gomperts, R.; Martin, R. L.; Fox, D. J.; Binkley, J. S.; Defrees, D. J.; Baker, J.; Stewart, J. P.; Head-Gordon, M.; Gonzalez, C.; Pople, J. A. Gaussian 94, Revision D.4; Gaussian, Inc.: Pittsburgh PA, 1995.

Table 2. Results for C_{60} Dimerization and Window Opening: Intermediates and Transition Structures

structure	symm	N_i[a]	R_a[b] (Å)	R_b[c] (Å)	MNDO level[d]	MNDO KK[e] (%)	MNDO LL[e] (%)	MNDO ΔH_f[f] (kcal/mol)	BLYP ΔE[g] (kcal/mol)
TS/Ia	D_{2h}	2[h]	2.137	2.137	HE-CI	56	44	63.0	51.9[i]
TS/Ib1	C_{2v}	2[j]	2.028	2.907	HE-CI	92	8	38.0	24.5
TS/Ib2	C_{2h}	1	2.037		HE-CI	94	6	34.8	16.6
TS/Ib3	C_2	1	2.037	3.227	HE-CI	94	6	34.4	18.9
C_{60}—C_{60} (**7a**)	C_{2v}	1[k]	1.576	2.744	HE-CI	52	48	16.9	33.9[l]
C_{60}—C_{60} (**7b**)	C_{2h}	0	1.578		HE-CI	60	40	14.5	27.8[m]
C_{60}—C_{60}	C_2	0	1.576	3.105	HE-CI	61	39	14.4	30.5[n]
TS/Ic	C_{2v}	1	1.561	2.461	HE-CI	72	28	17.8	31.5
C_{60}═C_{60} (**2**)	D_{2h}	0	1.560	1.560	S			−49.1	11.6
					HE-CI	100	0	−44.5[o]	
TS/IIa	D_{2h}	2[p]	2.224	2.224	HE-CI	53	47	37.1	82.6
TS/IIb	C_{2v}	1	2.040	2.649	HE-CI	76	24	28.0	86.7[q,r]
C_{60}⌒C_{60} (**3**)	D_{2h}	0	2.816	2.816	S			−13.4	75.5
					HE-CI	100	0	−9.4[o]	

[a] Number of imaginary frequencies. [b] Shorter of the breaking or forming bonds: Pivot bonds for **TS/Ia-Ts/Ic**, **2**, and **7**; hinge bonds for **TS/IIa**, **TS/IIb**, and **3**. [c] Longer of the breaking or forming bonds. [d] S = closed-shell SCF wave function. HE-CI = 3 × 3 CI using the singly occupied MOs of the half-electron open-shell singlet reference configuration. [e] Weights of the closed-shell configurations in the lowest CI state. KK (LL): The lower (upper) of the two singly occupied MOs of the reference configuration is doubly occupied. [f] Optimized MNDO heats of formation relative to two noninteracting C_{60} molecules. [g] Single-point BLYP/3-21G energies relative to two noninteracting C_{60} molecules computed at the optimized MNDO geometries. [h] Second imaginary mode (890*i* cm^{-1}) corresponds to a C_{2v} distortion. [i] Spin-polarized solution ($S^2 = 1.024$). Closed-shell solution at 56.6 kcal/mol. [j] Second imaginary mode (8*i* cm−1) corresponds to a C_2 distortion. [k] Imaginary mode (6*i* cm^{-1}) corresponds to a C_2 distortion. [l] Spin-polarized solution ($S^2 = 0.856$). Closed-shell solution at 35.7 kcal/mol. [m] Spin-polarized solution ($S^2 = 0.560$). Closed-shell solution at 28.4 kcal/mol. [n] Spin-polarized solution ($S^2 = 0.618$). Closed-shell solution at 31.1 kcal/mol. [o] Single-point calculation at the optimized MNDO closed-shell singlet geometry. [p] Second imaginary mode (640*i* cm^{-1}) leads to a C_{2v} distortion. [q] Spin-polarized solution ($S^2 = 1.021$). Closed-shell solution at 94.7 kcal/mol. [r] A geometry optimization of **TS/IIb** at the spin-unrestricted BLYP/3-21G level yields: $R_a = 2.16$ Å, $R_b = 2.61$ Å, $S^2 = 0.932$. **Ts/IIb** lies 83.0 kcal/mol above two noninteracting C_{60} molecules (BLYP/3-21G geometries).

("pivot") bonds. In the case of the dimer **2**, the experimental value for the gas phase heat of dimerization[69] appears to be reproduced well by the semiempirical methods and by LDA. The coincidence of the MNDO prediction (−49 kcal/mol) with the experiment (−48.2 ± 2.8 kcal/mol,[69] later adjusted to −46.8 ± 1.8 kcal/mol[70]) is probably fortuitous, since MNDO is known to overestimate the stability of the cyclobutane ring by about 18 kcal/mol.[48] The experimental value for the heat of dimerization may, however, have to be treated with caution, as the low intensity of the dimer signal makes verification of the pressure dependence of the equilibrium constant difficult.[70] Ab initio SCF and gradient-corrected DFT calculations predict **2** to be almost isoenergetic with two noninteracting C_{60} molecules, qualitatively consistent with the low estimated heats of depolymerization for high-pressure C_{60} phases.[25,28] The bonding situation in the high-pressure phases, however, is different from that in **2**, so that these solid-state results may not be directly comparable with those of the dimer.

For the window isomer **3** of the dimer, the semiempirical methods and BLYP/3-21G predict similar geometries with typical C═C double bonds in the intercage bridges. According to the semiempirical methods, **3** is approximately isoenergetic with two isolated C_{60} molecules (MNDO, −13 kcal/mol; AM1, +2 kcal/mol; PM3 + 11 kcal/mol). This result is intuitively understandable, since the number of formal single and double bonds is identical in two C_{60} molecules and in **3**. On the other hand, single-point ab initio and DFT calculations at the optimized MNDO geometries predict **3** to be significantly less stable than two isolated C_{60} molecules (e.g., BLYP/3-21G//MNDO, +76 kcal/mol), possibly reflecting residual strain around the cage junction.[41,47] This result remains qualitatively unchanged upon geometry relaxation at the DFT level (BLYP/3-21G, +70 kcal/mol) and basis set extension (BLYP/6-311G(d)//MNDO, +66 kcal/mol). This large discrepancy between semiempirical and DFT relative energies for **3** is surprising, since it has been demonstrated that the results obtained with these methods correlate very well for a wide range of fullerene structures[20,22,71] and there are no obvious reasons for the discrepancies in **3**.

Results for the dimerization reaction I and the window-opening step II are summarized in Table 2. At the MNDO/CI level, the symmetry-conserving stationary point **TS/Ia**, with an intercage separation of 2.137 Å, is 63 kcal/mol higher in energy than two C_{60} molecules. According to vibrational analysis, structure **TS/Ia** has a fully symmetric imaginary mode corresponding to the reaction I, but is unstable with respect to symmetry lowering from D_{2h} to C_{2v}. Relaxation of **TS/Ia** in the C_{2v} point group results in the structure **TS/Ib1** (38 kcal/mol above two C_{60} molecules). This is a second-order saddle point as well, with the smaller imaginary frequency (8*i* cm^{-1}) corresponding to a C_2 rotational distortion around the forming bond. Relaxation of this structure in C_2 symmetry lowers the energy further by 4 kcal/mol and produces the first-order saddle point **TS/Ib3** (see Figure 2).

Following the reaction coordinate from **TS/Ib3** leads to the single-bonded dimer **7c**, 14 kcal/mol above two C_{60} molecules, with a connecting bond of 1.576 Å (see Figure 1). **7c** is isoenergetic with the C_{2h} structure **7b**, which is usually considered for the single-bonded C_{60} dimer.[43,44] Since the barrier separating the two C_2 stereoisomers **7c** is very small (2.5 kcal/mol, TS **7a**; see Figure 2), the C_{60} moieties in the single-bonded dimer **7** should enjoy free rotation around the connecting bond. At the MNDO/CI level, **7c** is separated from the dimer **2** by a small barrier (**TS/Ic**, 3.4 kcal/mol above **7c**; see Figure 2), which is found at a distance of 2.461 Å for the second intercage bond. Given the small magnitude of this barrier, and a significant change in the configuration weights when going from **7c** to **TS/Ic**, this barrier may disappear with a more balanced treatment of static electron correlation.

(69) Korobov, M. V.; Dorozko, P. A.; Popov, A. A.; Filatova, G. N. In *Fullerenes*; Kadish, K. M., Ruoff, R. S., Eds.; Electrochemical Society: Pennington, 1996; Vol. 3, pp 491−500.

(70) Korobov, M. V. Personal communication, 1997.

(71) Cioslowski, J.; Patchkovskii, S.; Thiel, W. *Chem. Phys. Lett.* **1996**, *248*, 116−120.

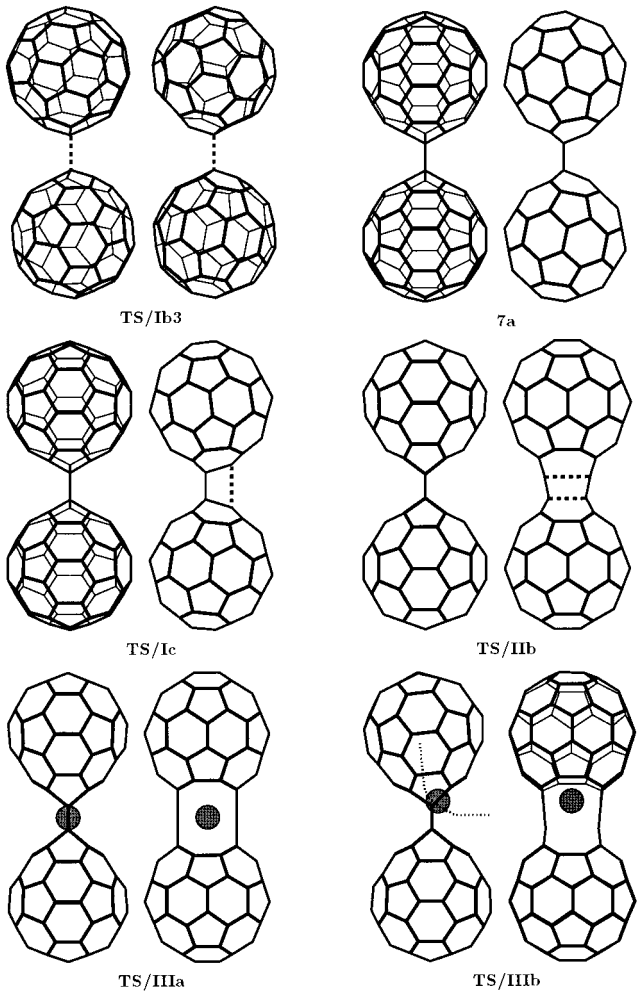

Figure 2. Optimized MNDO geometries for selected transition structures in the helium incorporation process. For each structure, left and front views are given. Forming or breaking bonds are indicated by dashed lines. The dotted line on the left view of **TS/IIIb** indicates the mass-weighted intrinsic reaction coordinate.

Due to the ready formation of the second intercage bond, the single-bonded isomer **7** is unlikely to be mechanistically important at elevated temperatures. The effective activation energy for the C_{60} dimerization reaction is thus determined by the transition state **TS/Ib3**, resulting in an MNDO activation barrier of 34 kcal/mol for dimerization. The MNDO barrier for the dissociation of the dimer **2** is considerably higher (83 kcal/mol, assuming the same transition structure as for dimerization). Adjusting this value downward by 18 kcal/mol (MNDO error in the heat of formation of cyclobutane) yields an estimate of 65 kcal/mol which is still significantly higher than the available experimental estimates (29 kcal/mol,[72] ~21 kcal/mol[34]) for analogous depolymerization processes in C_{60} photopolymers and high-pressure C_{60} phases.

The single-point BLYP results for the dimerization reaction I are qualitatively similar to the MNDO results in the sense that the least motion symmetric approach (via **TS/Ia**,) requires more activation (52 kcal/mol, BLYP; 63 kcal/mol, MNDO) than a less symmetric pathway (32 kcal/mol, BLYP; 34 kcal/mol, MNDO). In the latter case, however, the rate-determining step corresponds to the formation of the first new CC bond in MNDO (**TS/Ib3**) and to the formation of the second new CC bond in BLYP (**TS/Ic**). Moreover, the single-point BLYP energies provide no evidence for the existence of a single-bonded intermediate such as **7c**. These discrepancies in the details of the less symmetric pathway are not relevant for the overall mechanism and have therefore not been studied further (which would have required expensive BLYP geometry optimizations).

In the window-opening step II, MNDO locates the window isomer **3** of the dimer 36 kcal/mol higher in energy than the [2+2] dimer **2** (or 13 kcal/mol below two separated molecules). The corresponding D_{2h} stationary point **TS/IIa** (86 kcal/mol above **2**) is characterized by a separation of 2.224 Å between the hinge carbon atoms. In analogy to the dimerization reaction I, **TS/IIa** is unstable with respect to symmetry lowering from D_{2h} to C_{2v}. Following the symmetry-breaking imaginary mode leads to the C_{2v} transition structure **TS/IIb** (see Figure 2) which lies 9 kcal/mol below **TS/IIa**. The resulting MNDO activation barrier of 77 kcal/mol for the window-opening step II is probably overestimated due to the excessive stability of four-membered rings in MNDO. The reverse window closure reaction has an MNDO activation barrier of 41 kcal/mol, assuming the same reaction path.

At the BLYP//MNDO level, the window isomer **3** is significantly less stable than either the dimer **2** (by 64 kcal/mol) or two C_{60} molecules (by 76 kcal/mol). Given the large difference between the MNDO and BLYP heats of reaction for step II (36 vs 64 kcal/mol), the transition structure is expected to occur later on the reaction path in BLYP than in MNDO, so that the single-point BLYP energies for **TS/IIa** and **TS/IIb** (Table 2) are probably not too meaningful. The geometry of the transition state **TS/IIb** has therefore been reoptimized at the BLYP level which yields BLYP barriers of 13 kcal/mol for window closure (**3** → **2**) and 75 kcal/mol for window opening (**2** → **3**).

Results for the noble gas incorporation step III are summarized in Table 3. According to MNDO, the window isomer **4** with He inside one of the C_{60} fragments (see Figure 1) is 5 kcal/mol above separated He and **3**. Since MNDO is known to overestimate the energy of He inside C_{60} by about 5 kcal/mol,[49] the actual reaction enthalpy for step III should be close to zero.

Placing He at the inversion center of **3** results in the second-order saddle point **TS/IIIa** (see Figure 2), which is 109 kcal/mol higher in energy than noninteracting He and **3**. The distance between the two carbon bridges in **TS/IIIa** is 3.37 Å; i.e., they are 0.56 Å farther apart than in **3**, indicating a very flexible window. According to single-point MNDO calculations, 29 kcal/mol of the barrier is due to the increased window width. The rest (80 kcal/mol) is attributable to the interactions with the helium atom. The larger of the two imaginary frequencies in **TS/IIIa** ($547i$ cm^{-1}) corresponds to separation of He and **3**. Following the second imaginary mode ($400i$ cm^{-1}) moves the helium atom into one of the connected C_{60} cages.

The true MNDO transition structure for the incorporation reaction III, **TS/IIIb** (see Figure 2), has C_s symmetry, and is 97 kcal/mol above noninteracting He and **3**. In **TS/IIIb**, the CC distance corresponding to the window-forming hinge bond in the C_{60}, fragment receiving He is markedly longer (3.248 Å) than the corresponding distance (3.059 Å) in the second half of the dimer. The mass-weighted intrinsic reaction coordinate path going through the transition structure **TS/IIIb** (see Figure 2) is fairly unusual, as the direction of the He motion changes by almost 90° between reactants and products. As a consequence, a strong temperature dependence of the effective Arrhenius activation energy may be expected for this reaction.

(72) Wang, Y.; Holden, J. M.; Bi, X.-X.; Eklund, P. C. *Chem. Phys. Lett.* **1994**, *217*, 413−417.

Table 3. Results for He and Ne Incorporation into the Window Isomer **3**

structure	symm	level	N_i[a]	R_a[b] (Å)	R_b[c] (Å)	ΔE[d] (kcal/mol)
He@C_{60}⌒C_{60} **(4)**	C_{2v}	MNDO	0	2.816	2.815	−8.4
		BLYP//MNDO		2.816	2.815	74.6
C_{60}⌒C_{60} + He **(TS/IIIa)**	D_{2h}	MNDO	2	3.373		95.7
		BLYP//MNDO		3.373		193.2
		BLYP		3.497		186.4
C_{60}⌒C_{60} + He **(TS//IIIb)**	C_s	MNDO	1	3.248	3.059	83.9
		BLYP//MNDO		3.248	3.059	150.2
		BLYP		3.160	2.730	138.4
C_{60}⌒C_{60} + Ne **(TS/IIIa-Ne)**	D_{2h}	BLYP//MNDO[e]		3.373		249.3
		BLYP		3.767		213.5
C_{60}⌒C_{60} + Ne **(TS/IIIb-Ne)**	C_s	BLYP//MNDO[e]		3.248	3.059	217.9
		BLYP		3.642	3.138	185.2

[a] Number of imaginary frequencies. [b] Larger of the hinge C···C distances. [c] Smaller of the hinge C···C distances. [d] Relative to two noninteracting C_{60} molecules and a noble gas atom. [e] Evaluated at the MNDO geometry of the corresponding transition structure for helium.

The single-point BLYP//MNDO results for step III are in fair agreement with the MNDO results. Thus, the D_{2h} saddle point **TS/IIIa** and the C_s structure **TS/IIIb** are 118 and 75 kcal/mol, respectively, above separated He and **3** (MNDO: 109 and 97 kcal/mol). Geometry optimization at the BLYP/3-21G level lowers the relative energy of **TS/IIIa** by 1.2 kcal/mol, while **TS/IIIb** is stabilized by 6.2 kcal/mol. Such relatively small changes in the reaction barriers, despite significant changes in the window width (0.12 Å for **TS/IIIa**, 0.09 Å for **TS/IIIb**), are not surprising, given the flexibility of the window.

Any mechanism proposed for helium incorporation should ideally also account for the incorporation of heavier noble gases. Therefore, we have computed the BLYP/3-21G activation barriers for neon incorporation. Optimized geometries of the D_{2h} **TS/IIIa-Ne** and C_s **TS/IIIb-Ne** stationary points are qualitatively similar to their helium counterparts, with the window widths increased by 0.27 Å (**TS/IIIa-Ne**) and 0.48 Å (**TS/IIIb-Ne**), respectively. Their energies are somewhat higher than in the helium case (**TS/IIIa-Ne**, 144 kcal/mol; **TS/IIIb-Ne**, 115 kcal/mol, relative to noninteracting **3** and Ne). Because of the increased atom size, the results for Ne should be more sensitive to the presence of polarization functions in the basis than those for He. Therefore, the barrier of 115 kcal/mol for Ne inclusion through the window **3** is likely to decrease further upon basis set extension. Such a barrier would seem compatible with the experimental observations for Ne.[21]

In the two remaining reaction steps, namely, window closure (IV) and dissociation of the filled dimer (V), the noble gas atom does not come into close contact with the reactive centers. Reactions IV and V are then essentially the reverse of the processes II and I. Indeed, MNDO calculations on the corresponding intermediates and transition structures lead to completely analogous geometries and to a uniform increase in the heat of formation by 5 kcal/mol (i.e., the MNDO energy difference[49] between He@C_{60} and noninteracting He and C_{60}). Hence, there is no need to present these MNDO data or to study the reactions IV and V with density functional methods.

Given the crucial significance of the C_{60} dimer **2** and its window isomer **3** for the proposed mechanism of noble gas incorporation, it is interesting to examine the spectral features which may assist in their experimental identification.

Simulated MNDO and RHF/3-21G ^{13}C NMR spectra of **2** and **3**, computed at the optimized MNDO geometry relative to free C_{60},[73] are shown in Figure 3. The MNDO predictions for the dimer **2** agree reasonably well with the experimental findings

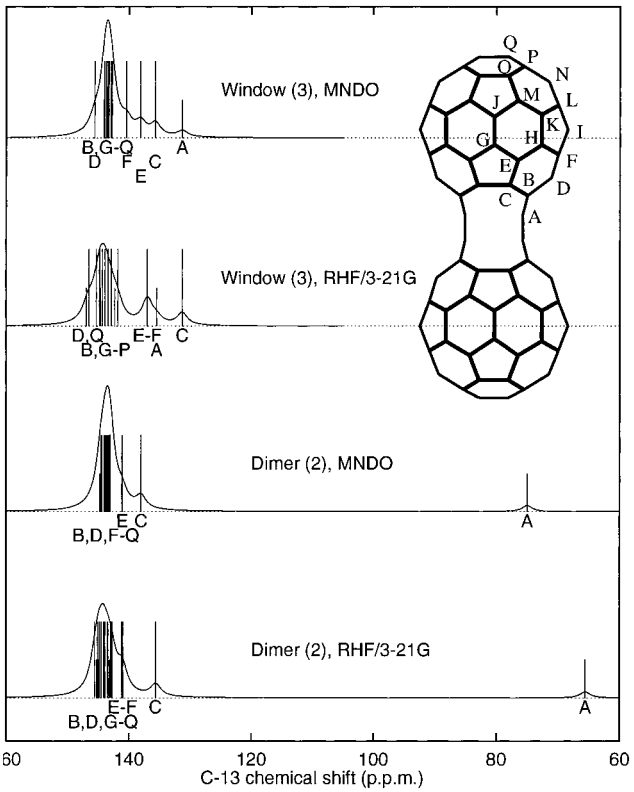

Figure 3. Calculated NMR spectra of the C_{60} dimer **2** and its window isomer **3**. Simulated envelopes were produced using Lorentzian line shapes with a half-width of 1 ppm. Free C_{60} was used as a reference (exptl δ = 142.7 ppm[73]).

for the linear C_{60} polymer and dimer **2**, with a broad sp^2 signal at 144 ppm (experiment: 144,[28,33] 146,[35] 139.02−151.42[37] ppm) and an sp^3 signal at 75 ppm (experiment: 77,[28,33] 73.5,[35] 76.22[37] ppm), even though the fine structure of the signal of the sp^2 core[37] is not well reproduced by MNDO. At the ab initio RHF/3-21G level, the sp^2 signals are predicted in the 135−145 ppm range, while the sp^3 carbons appear at 66 ppm. The latter value is too small by 10 ppm compared with experiment,[37] probably because the 3-21G basis is not sufficiently flexible to describe ^{13}C shielding adequately. In the window form of the dimer, the sp^3 peak disappears, while several sp^2 signals move upfield by up to 15 ppm from the poorly resolved multiplet of the C_{60} cores. Although the exact shape of the signal depends on the theoretical method used, the NMR spectra of **2** and **3** appear sufficiently different to allow the experimental identification of the window dimer **3**.

(73) Taylor, R.; Hare, J. P.; Abdul-Sada, A. K.; Kroto, H. W. *J. Chem. Soc., Chem. Commun.* **1990**, 1423−1425.

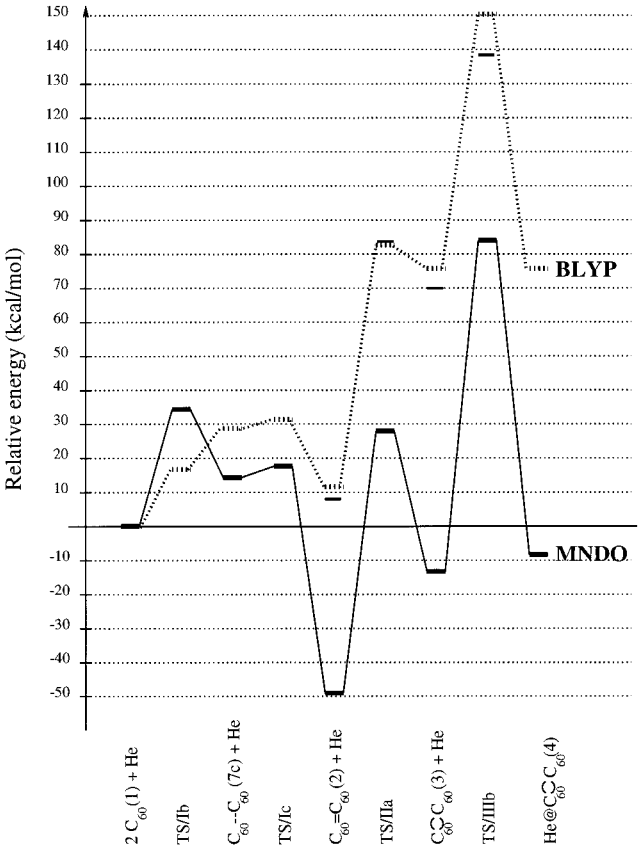

Figure 4. Schematic reaction diagram of the dimer route for helium incorporation into C_{60}. Heats of formation (MNDO) and single-point energies (BLYP//MNDO) are given relative to two C_{60} molecules and He at infinite separation. Solid lines close to the dashed BLYP//MNDO path correspond to BLYP energies at optimized BLYP geometries.

For the analysis of the infrared and Raman spectra, MNDO vibrational frequencies were uniformly scaled by 0.886. This scaling results in an rms deviation of 39 cm^{-1} from the experimental values[36,74,75] for the 14 (10 Raman and 4 IR) symmetry-allowed vibrational transitions of pristine C_{60}. There is qualitative agreement between the experimental[23−25,28,30,33,36,37,76] vibrational frequencies for various C_{60} polymers and the scaled MNDO results for dimer **2**, particularly for the bands derived from the dipole-allowed modes of C_{60}, the interball Raman mode, and the pentagonal pinch mode. Upon formation of the window isomer **3**, significant changes occur in the simulated spectra. Most importantly, a pair of IR (B_{3u}) and Raman (A_g) active modes appears in the spectra of **3** at 1700 cm^{-1}, well outside the normal range for pristine C_{60} and C_{60} polymers. Upon visual inspection, these modes can be classified as anti-phase (B_{3u}) and in-phase (A_g) vibrations of the connecting C═C double bonds, largely uncoupled from the cage motions. More details and plots of the simulated spectra are given in the Supporting Information.

Discussion

The overall reaction profile for the proposed mechanism of helium incorporation is shown in Figure 4, for both MNDO and BLYP//MNDO. Since there are qualitative differences, the MNDO and BLYP results will be discussed separately.

According to MNDO, four fairly stable intermediates (dimer **2**, window **3**, He in window **4**, and He in dimer **5**) appear on the reaction path. The effective activation barriers of the elementary reactions are comparable to each other (dimerization I, 34 kcal/mol; window opening II, 77 kcal/mol; He insertion III, 97 kcal/mol; window closure IV, 41 kcal/mol; dimer dissociation V, 84 kcal/mol), and compatible with the high-pressure experiments.[7−9] Two of the higher MNDO barriers (reactions II and V) are probably overestimated by about 18 kcal/mol due to the excessive stability of cyclobutane in MNDO.[48] Given the similar magnitude of the barriers, the rate-limiting step may well be determined by entropic factors and reaction conditions. However, the overall effective activation energy should not exceed 100 kcal/mol.

At the BLYP//MNDO level, only two intermediates are of sufficient kinetic stability to be mechanistically relevant at elevated temperatures: dimer **2** and He in dimer **5**. According to BLYP calculations at optimized BLYP geometries, the barrier to closure of the window dimer is 13 kcal/mol. Hence, **3** should not be stable in the high-pressure experiments ($RT = 1.8$ kcal/mol at 600 °C). In this case, the activation barriers for the elementary reactions (dimerization I, 32 kcal/mol; He insertion II + III + IV, 139 kcal/mol; dimer dissociation V, 20 kcal/mol) would then differ enough to make helium insertion the rate-limiting step. The BLYP//MNDO barrier of 139 kcal/mol compares favorably to the analogous barriers in C_{60} (≥200 kcal/mol[20]), $C_{60}CH_3$ (≥160 kcal/mol[22]), and $C_{60}(CH_3)_2$ (∼130−140 kcal/mol[22]). It is lowered to 130 kcal/mol by reoptimizing the geometries at the BLYP level (see entries for **2** and **TS/IIIb** in Tables 1 and 3, respectively) and may further be reduced slightly at higher theoretical levels.[20] Even so, this barrier remains fairly high, and would probably not account for the experimental results.[7−9] Using neon, instead of helium, leads to a barrier of 115 kcal/mol (BLYP/3-21G) for the insertion reaction III, and to an overall effective BLYP barrier of 177 kcal/mol. Only the former value would seem compatible with the experimental observations on neon release.[21]

The discrepancies between the MNDO and BLYP conclusions for the reaction mechanism are due to the different stability computed for the dimer **2** (MNDO, −49 kcal/mol; BLYP, +8 kcal/mol) and its window isomer **3** (MNDO, −13 kcal/mol; BLYP, +70 kcal/mol) relative to two isolated C_{60} molecules. The available experimental evidence is ambiguous, and does not allow selection of either set of theoretical results over the other. Thus, the gas-phase heat of C_{60} dimerization (−48 kcal/mol[69]) is consistent with MNDO, but not with BLYP. The solid-state effective barriers for dimer dissociation (21−29 kcal/mol[34,72]) are consistent with BLYP, but not with MNDO. Finally, the solid-state heat of depolymerization (≥0[25,28]) may be reconciled with both the MNDO and BLYP results. High-level correlated ab initio computations might help to resolve these discrepancies. However, such computations are presently not feasible for **2** and **3** (D_{2h} symmetry, 120 atoms, 1080 basis functions with 3-21G, 2160 basis functions with 6-311G(d)), or for a meaningful truncated model of these structures.

An experimental observation of the window isomer **3** would be the most direct experimental confirmation of the proposed mechanism. With an MNDO barrier of 41 kcal/mol for window closure, the closed-shell window dimer **3** may be sufficiently stable at ambient conditions to allow its spectra to be taken. If the barriers for dissociation of the dimer **2** and for window opening are of comparable magnitude, as indicated by MNDO, it may be possible to isolate the window isomer from polym-

(74) Lynch, K.; Tanke, C.; Menzel, F.; Brockner, W.; Scharff, P.; Stumpp, E. *J. Phys. Chem.* **1995**, *99*, 7985−7992.
(75) Holleman, I.; Boogaarts, M. G. H.; van Bentum, P. J. M.; Meijer, G. *Chem. Phys. Lett.* **1995**, *240*, 165−171.
(76) Rao, A. M.; Eklund, P. C.; Hodeau, J.-L.; Marques, L.; Nunez-Regueiro, M. *Phys. Rev. B* **1997**, *55*, 4766−4773.

erized samples quenched while undergoing thermal decomposition. With the distinctive pattern of the sp^2 signals in the ^{13}C NMR spectrum, and the high-frequency C═C stretching modes in Raman and IR spectra, the window dimer **3** should then be easily identifiable.

In the high-pressure experiments,[7−9] several noble gases (He, Ne, Ar, Kr) can be incorporated into C_{60} with similar yields (ca. 0.1%). According to the BLYP/3-21G calculations, the barrier for the insertion into the window dimer **3** increases from 69 to 115 kcal/mol when replacing He by Ne. Even though the addition of polarization functions should lower the second value more than the first one, the barrier for Ne is expected to remain higher than for He, and it seems qualitatively reasonable to assume still higher barriers for Ar and Kr. By implication, the insertion of the heavier noble gases may require larger windows (which have not been studied presently). This argument applies to any window mechanism regardless of whether monomers or dimers of C_{60} are involved. In this context, the present calculations indicate that window-type structures and transition states are energetically more accessible in the dimer than in the monomer.

Experimentally, the low yield of endohedral products such as Ne@C_{60} cannot be increased by longer reaction times.[9,21] However, if these endohedral compounds are isolated and relabeled, the noble gas content is approximately doubled.[9,21] This has been ascribed to an unknown "promoter" which is used up during the reaction.[77] Such a promoter could also operate in the dimer mechanism (even though this may seem unlikely), but there is a second possibility: Judging from the published phase diagram (*p*, *T*) of C_{60},[78,79] small quantities of C_{60} dimers and oligomers may be synthesized during early stages of the high-pressure treatment,[7−9] while the temperature of the sample is still below the dimer dissociation threshold (ca. 160 °C at ambient pressure[26,37]). Once the temperature is raised, window opening would compete with the dimer dissociation, thus limiting the total yield to a fraction of the original amount of the dimer, regardless of the reaction time. Hence, in a sense, the C_{60} dimers generated in situ would play the role of a promoter. To explore this idea, it would be interesting to subject a bulk polymerized C_{60} sample (e.g., from high-pressure high-temperature experiments[25,28−30]) or a sample of the pure dimer **2**[37] to a high noble gas pressure at a temperature slightly above the dissociation threshold.

In principle, helium incorporation via dimers could also occur in higher fullerenes, such as C_{70}. Although C_{70} does not polymerize at high pressure,[80] and polymerizes very slowly under irradiation with UV or visible light,[81] this behavior is probably due to crystal packing effects,[81] rather than to an intrinsic lack of reactivity. Indeed, C_{70} polymerizes readily in the gas phase[69] or upon UV irradiation[27] in solution. Cross-polymerization with C_{60} should also be possible, even in mixed solid phases, due to free rotation of the C_{60} molecule at elevated temperatures.

Another interesting possibility is noble gas inclusion by other fullerene derivatives containing the same dimer motif. If C_{60} cages in such compounds are connected by other substituents in addition to the cyclobutane bridge, as in $C_{120}O_2$,[82] additional bonds may inhibit the thermal dissociation without interfering with the window-opening step. Such tethered dimers may survive the conditions of the high-pressure treatment[7−9] long enough to achieve equilibrium with the substance to be incorporated. With the theoretically predicted equilibrium He@C_{60}/C_{60} ratios exceeding 10%,[17,18] a few percent of the dimers could end up with a noble gas atom in each of the two cages.

Conclusions

An autocatalytic mechanism for helium incorporation into buckminsterfullerene has been examined which involves the formation of a [2+2] C_{60} dimer **2**, ring opening to a stable closed-shell window isomer **3**, and the insertion of helium through this window. According to MNDO, the activation barriers do not exceed 100 kcal/mol for any of these reaction steps. At the BLYP//MNDO level, the window isomer **3** seems kinetically less stable and may therefore be mechanistically less relevant, which would imply an effective BLYP barrier for helium incorporation of about 130 kcal/mol (relative to **2**). If the closed-shell window intermediate **3** is sufficiently stable to be isolated experimentally, it should be easily detectable from a characteristic ^{13}C NMR spectrum and the high-frequency C═C stretching modes in the IR and Raman spectra. The dimer mechanism could also apply to the inclusion of other noble gases by buckminsterfullerene and to higher fullerenes such as C_{70}. It suggests novel approaches to the synthesis of fullerenes with a noble gas atom inside, namely incorporation of guests by polymeric C_{60} phases and by tethered C_{60} dimers.

Acknowledgment. This work was supported by the Schweizerischer Nationalfonds. Parts of the computations were performed at the Competence Center for Computational Chemistry (C4) at ETH Zürich.

Supporting Information Available: Total energies and heats of formation for the C_{60} dimer **2** and its window isomer **3**, and infrared and Raman spectra of the dimers **2** and **3** (3 pages). See any current masthead page for ordering and Internet access instructions.

JA972456V

(77) Saunders, M. Personal communication, 1997.
(78) Bashkin, I. O.; Rashchupkin, V. I.; Gurov, A. F.; Moravsky, A. P.; Rybchenko, O. G.; Kobelev, N. P.; Soifer, Ya. M.; Ponyatovsky, E. G. *J. Phys. Condens. Matter* **1994**, *6*, 7491−7498.
(79) Davydov, V. A.; Kashevarova, L. S.; Rakhmanina, A. V.; Agafonov, V. N.; Ceolin, R.; Szwarc, H. *JETP Lett.* **1996**, *63*, 818−824.
(80) Sundar, C. S.; Sahu, P.Ch.; Sastry, V. S.; Rao, G. V. N.; Sridharan, V.; Premila, M.; Bharathi, A.; Hariharan, Y.; Radhakrishnan, T. S.; Muthu, D. V. S.; Sood, A. K. *Phys. Rev. B* **1996**, *53*, 8180−8183.
(81) Rao, A. M.; Menon, M.; Wang, K.-A.; Eklund, P. C.; Subbaswamy, K. R.; Cornett, D. S.; Duncan, M. A.; Amster, I. J. *Chem. Phys. Lett.* **1994**, *224*, 106−112.
(82) Gromov, A.; Lebedkin, S.; Ballenweg, S.; Avent, A. G.; Taylor, R.; Krätschmer, W. *J. Chem. Soc., Chem. Commun.* **1997**, 209−210.
(83) Cartesian coordinates and MNDO normal vibrational modes for all structures are available from the authors on request.